Kirchhoff prestack depth scalar migration of complete wave fields in a simple velocity model with triclinic anisotropy: PP, PS1 and PS2 waves

Václav Bucha
Department of Geophysics, Faculty of Mathematics and Physics, Charles University, Ke Karlovu 3, 121 16 Praha 2, Czech Republic, bucha@seis.karlov.mff.cuni.cz

Summary

We test 3-D ray-based Kirchhoff prestack depth scalar migration and calculate migrated sections in a simple anisotropic velocity model. The velocity model is composed of two homogeneous layers separated by a curved interface. The upper layer has triclinic anisotropy and the bottom layer is isotropic. The synthetic complete seismic wave field is calculated using the Fourier pseudospectral method. We apply a scalar imaging to each component of the complete wave field in a single-layer velocity model with the same triclinic anisotropy as in the upper layer of the velocity model used to calculate the recorded wave field. We display and discuss resulting migrated sections.

Keywords

Fourier pseudospectral method, 3-D Kirchhoff prestack depth scalar migration, anisotropic velocity model, triclinic anisotropy, complete wave field

1. Introduction

In the papers by Bucha (2018b, 2019a) we migrated a complete wave field calculated by the Fourier pseudospectral method (Tessmer, 1995) in the velocity models with inhomogeneous weak anisotropy (QI, QI4). For imaging of the S-wave part of the converted PS wave we compared three methods: common S-wave approximation, the anisotropic-ray-theory approximation of S waves, and the prevailing-frequency approximation of the coupling ray theory for S waves (Klimeš & Bulant, 2016). In spite of complex recorded wave fields, the migrated interfaces were in all stacked migrated sections relatively good with exception of spurious interface images close to the correct ones for converted PS1 and PS2 waves. To verify the relatively good imaging results, we test in this paper migration of the complete wave field calculated in the velocity model with triclinic anisotropy.

The dimensions of the velocity model and the shot-receiver configuration are the same as in the previous papers by Bucha (e.g., 2012, 2013, 2017, 2018a), where we studied the migration problems with incorrect anisotropy, incorrect gradients or incorrect rotation of the stiffness tensor, three-component elastic scalar imaging.

To compute the synthetic recorded wave field, we use simple anisotropic velocity model composed of two homogeneous layers separated by one curved interface that is non-inclined in the direction perpendicular to the source-receiver profiles. The upper layer has triclinic anisotropy and the bottom layer is isotropic. The velocity model for calculation of the complete wave field by the Fourier pseudospectral method is extended by absorption stripes at the sides.

Seismic Waves in Complex 3–D Structures, **30** (2020), 29–40 (ISSN 2336–3827, online at http://sw3d.cz)

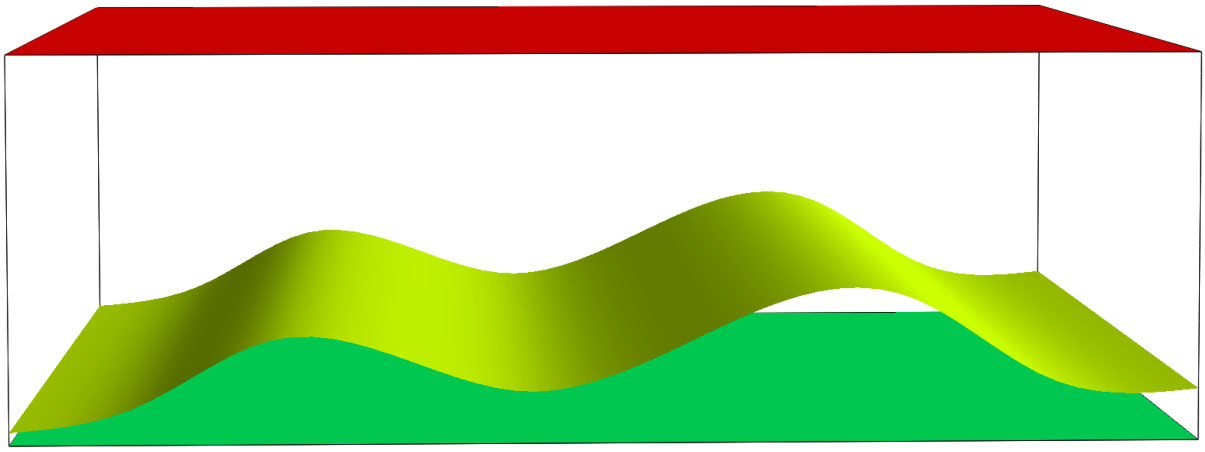

Figure 1. Velocity model with a curved interface which is non-inclined in the direction perpendicular to the source-receiver profiles. The horizontal dimensions of the velocity model are 0 km $\leq x_1 \leq$ 9.2 km, 0 km $\leq x_2 \leq$ 10 km and the depth is 0 km $\leq x_3 \leq$ 3 km.

We then migrate complete wave field using 3-D ray-based Kirchhoff prestack depth scalar migration in the single-layer velocity model with triclinic anisotropy. Under the scalar migration, we understand here the migration of just a single component of the recorded elastic wave field. The elastic moduli in the velocity model used for migration correspond to the upper layer of the velocity model in which the synthetic recorded seismograms have been calculated. For migration we utilize the MODEL, CRT, FORMS and DATA software packages (Červený, Klimeš & Pšenčík, 1988; Bulant, 1996; Bucha & Bulant, 2019). S1 and S2 parts of converted PS1 and PS2 waves are computed using anisotropic-ray-theory method.

2. Velocity model and measurement configuration

The dimensions of the velocity model and the measurement configuration are derived from the 2-D Marmousi model and dataset (Versteeg & Grau, 1991). The recorded wave field is computed in the velocity model composed of two homogeneous layers separated by one curved interface (see Figure 1). The curved interface is non-inclined in the direction of the x_2 axis which is perpendicular to the source-receiver profiles. The medium in the upper layer is triclinic and the bottom layer is isotropic.

The triclinic medium is represented by dry Vosges sandstone (Mensch and Rasolofosaon 1997). Triclinic anisotropy is asymmetric, there are no mirror planes and no axes of symmetry. The matrix of density-reduced elastic moduli in $\mathrm{km}^2/\mathrm{s}^2$ reads

$$\begin{pmatrix} 10.3 & 0.9 & 1.3 & 1.4 & 1.1 & 0.8 \\ & 10.6 & 2.1 & 0.2 & -0.2 & -0.6 \\ & & 14.1 & 0.0 & -0.5 & -1.0 \\ & & & 5.1 & 0.0 & 0.2 \\ & & & & 6.0 & 0.0 \\ & & & & & 4.9 \end{pmatrix}. \tag{1}$$

The values of anisotropy strength, defined as $2(P_{max} - P_{min})/(P_{max} + P_{min}) \times 100\%$, where P_{min} and P_{max} are minimum and maximum absolute norms of the slowness vector, are 21.2 % for P wave, 17.0 % for S1 wave and 19.7 % for S2 wave. The P

wave velocity in the isotropic bottom layer is $V_p = 3.6$ km/s and the S wave velocity is $V_s = V_p/\sqrt{3}$.

We migrate in the single-layer velocity model (without the interface) with the same triclinic anisotropy given by matrix (1). The elastic moduli in the velocity model correspond to the upper layer of the velocity model in which the synthetic data have been calculated.

The profile lines are parallel with the x_1 coordinate axis (see Figure 2). Each profile line has the following configuration: The first shot is 3 km from the left-hand side of the velocity model, the last shot is 8.975 km from the left-hand side of the velocity model, the distance between the shots is 0.025 km, and the depth of the shots is 0 km. The total number of shots along one profile line is 240. The number of receivers per shot is 96, the first receiver is located 2.575 km left of the shot location, the last receiver is 0.2 km left of the shot location, the distance between the receivers is 0.025 km, and the depth of the receivers is 0 km. This configuration simulates a simplified towed streamer acquisition geometry. The 3-D measurement configuration consists of 81 parallel profile lines (see Figure 2). The interval between the parallel profile lines is 0.025 km.

3. Recorded wave field

To calculate the recorded wave field for 240 shots, we apply code FT43DANX by E. Tessmer (Tessmer, 1995). The code is based on the Fourier method (FM), a kind of pseudospectral method (e.g., Kosloff & Baysal, 1982). The code FT43DANX was previously used to test the accuracy of coupling ray theory and standard ray theory results in 3-D inhomogeneous, weakly anisotropic media without interfaces (Pšenčík, Farra & Tessmer, 2011; Bulant et al., 2011). This implementation of the FM is applicable to any type and strength of anisotropy. It works equally well in regular as well as in singular regions of the ray method.

The algorithm is based on a regular numerical grid. For simple structures with horizontal layering, the input parameters for velocity model are located in the main ASCII input file. The velocity model for our tests contains a curved interface. In such a case, the input structure for code FT43DANX needs to be gridded and saved in a separate binary file. We performed gridding of the velocity model using the MODEL and FORMS packages (Červený, Klimeš & Pšenčík, 1988; Bucha & Bulant, 2019). There are two limitations for setting grid sizes. The first is that the grid size numbers must be factorizable into the factors up to 23, and the FFT algorithm is the more efficient the smaller factors are. The second limitation is connected with the first one, the grid sizes must be odd numbers.

To avoid wrap-around or boundary reflections, the model is surrounded by sponge-like absorbing regions (Cerjan et al., 1985). This requires the numerical grid to be extended at its sides. We present calculation with 20 absorption grid points at the sides of the model (see Figure 3). The enlarged model has numerical grid $405 \times 165 \times 189$ grid nodes in the x_1, x_2 and x_3 directions, respectively. The grid steps are 0.025 km.

We use an explosive source for calculating the synthetic seismograms. The source-time function is a Gabor wavelet, $\exp[-(2\pi f/\gamma)^2 2t^2]\cos(2\pi f t)$, with the dominant frequency $f = 25$ Hz and $\gamma = 4$. The time step for wave field calculation is 0.004 s and the propagation time starts at 0 s and ends at 2.5 s. The source must be away from the surface. Sources and receivers should be at least 5 grid points away from the absorbing boundaries. Source and receiver positions are specified by grid indices.

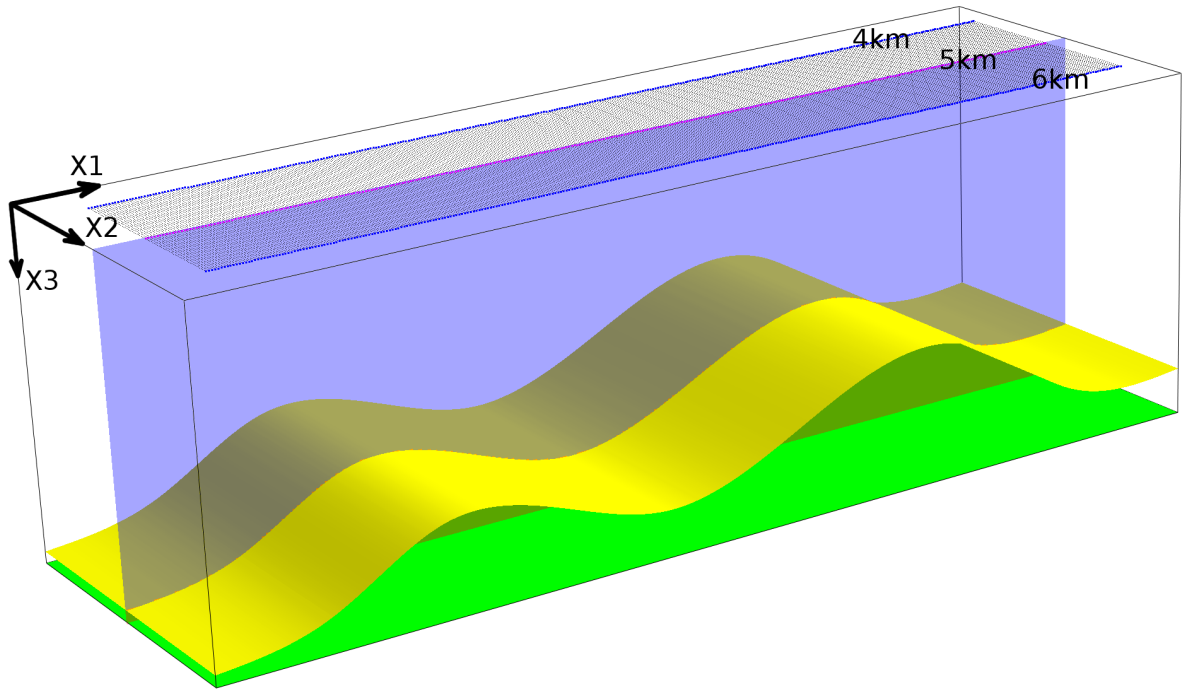

Figure 2. Part of the velocity model with 81 parallel profile lines, the curved interface (yellow) and the bottom velocity model plane (green). The horizontal dimensions of the depicted part of the velocity model are 0 km $\leq x_1 \leq$ 9.2 km, 3.5 km $\leq x_2 \leq$ 6.5 km, the depth is 0 km $\leq x_3 \leq$ 3 km. We compute and stack migrated sections in the 2-D plane (blue) located in the middle of the shot-receiver configuration, at horizontal coordinate $x_2 = 5$ km.

Due to the above mentioned limitations and requirements, it is not easy to find the suitable computational grid parameters. Moreover, numerical algorithms based on pseudospectral methods are computationally more expensive than finite-difference methods. We tested the Fourier method with various values of input parameters. The results in the paper correspond to our best selection up to date.

The recorded wave field is equal for all parallel profile lines, because the distribution of elastic moduli in the upper layer is homogeneous, the bottom layer is homogeneous, and the non-inclined curved interface is independent of the coordinate x_2 perpendicular to the profile lines (2.5-D velocity model, see Figures 1 and 2).

The Fourier method calculates many waves in regions where the ray-theory method fails. For plotting Fourier method (FM) seismograms, we use the Seismic Unix plotting tools (Cohen & Stockwell, 2013). Seismograms are calculated and plotted up to the time of 2.5 s. Figure 4 displays the three-component complete wave field for common-shot gather 1 calculated in the velocity model with triclinic anisotropy in the upper layer.

4. Kirchhoff prestack depth scalar migration

We use the MODEL, CRT, FORMS and DATA software packages for the ray-based 3-D Kirchhoff prestack depth scalar migration (Červený, Klimeš & Pšenčík, 1988; Bulant, 1996; Bucha & Bulant, 2019). We migrate the complete wave field without decomposition.

The ray-based migration consists of two-parametric controlled initial-value ray tracing (Bulant, 1999) from the individual surface points, calculating the grid values of travel times and amplitudes by interpolation within ray cells (Bulant & Klimeš, 1999; Klimeš

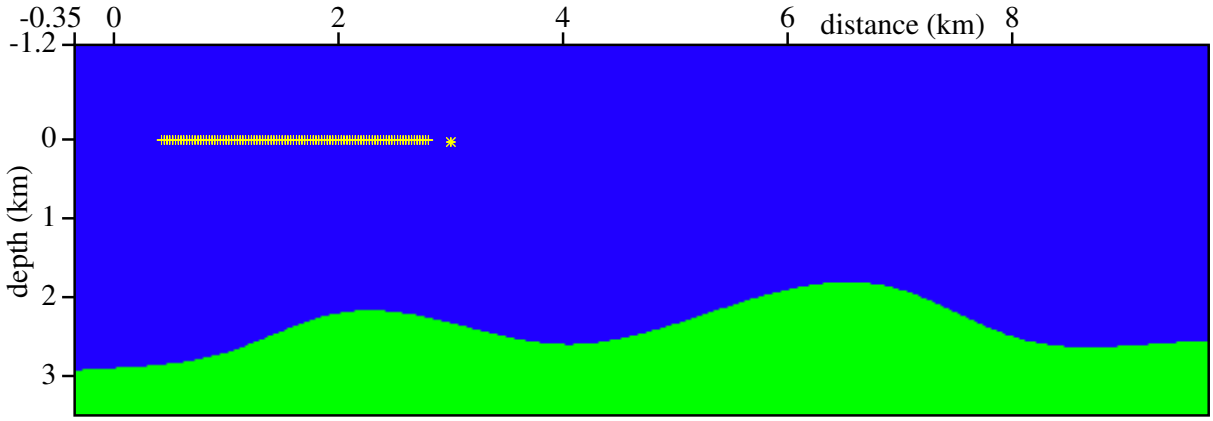

Figure 3. Section of the enlarged velocity model with 20 absorption grid points for the FM calculation. The dimensions of the section are -0.35 km $\leq x_1 \leq 9.75$ km and -1.2 km $\leq x_3 \leq 3.5$ km. We display common-shot gather 1. Note the stepwise discretization of the smooth interface.

& Bulant, 2017), performing the common-shot Kirchhoff migration and stacking the migrated images. The shot-receiver configuration consists of 81 parallel profile lines at intervals of 0.025 km (see Figure 2). The first profile line is situated at horizontal coordinate $x_2 = 4$ km and the last profile line is situated at horizontal coordinate $x_2 = 6$ km. For migration we use the single-layer velocity model (without the curved interface) with the same triclinic anisotropy as in the upper layer of the velocity model used to calculate the recorded wave field, given by matrix (1).

In our tests, we calculate only one vertical image section corresponding to the central profile line ($x_2 = 5$ km, see Figure 2). Although it is only a 2-D profile line, such an image represents one vertical section of a full 3-D migrated volume. We form the image by computing and summing the corresponding contributions (images) from all 81 parallel source-receiver lines. While summing the contributions, the constructive interference focuses the migrated interface and the destructive interference reduces undesirable migration artefacts (non-specular reflections). We also use cosine taper to clear artefacts, but some of them remain.

In the ray-based 3-D Kirchhoff prestack depth scalar migration, we decompose both the incident wave field and the back-propagated recorded wave field into elementary waves P, S1 and S2. In this paper, we refer to the faster S wave as the S1 wave, and to the slower S wave as the S2 wave. If we migrate with the incident P wave and the back-propagated P wave, we speak about migrating the PP reflected wave, although we migrate the complete recorded wave field. Analogously, if we migrate with the incident P wave and the back-propagated S2 wave, we speak about migrating the PS2 converted wave. The migration is tested for radial (X1), transversal (X2) and vertical (X3) components of the PP reflected wave, PS1 and PS2 converted waves. S1 and S2 parts of converted waves are calculated using anisotropic-ray-theory method. The computations are performed in the homogeneous triclinic velocity model defined by matrix (1). Migrated sections displayed in this paper have stair-step interfaces caused by gridded velocity models. For detailed explanation of the stair-step problem, please refer to Bucha (2019b).

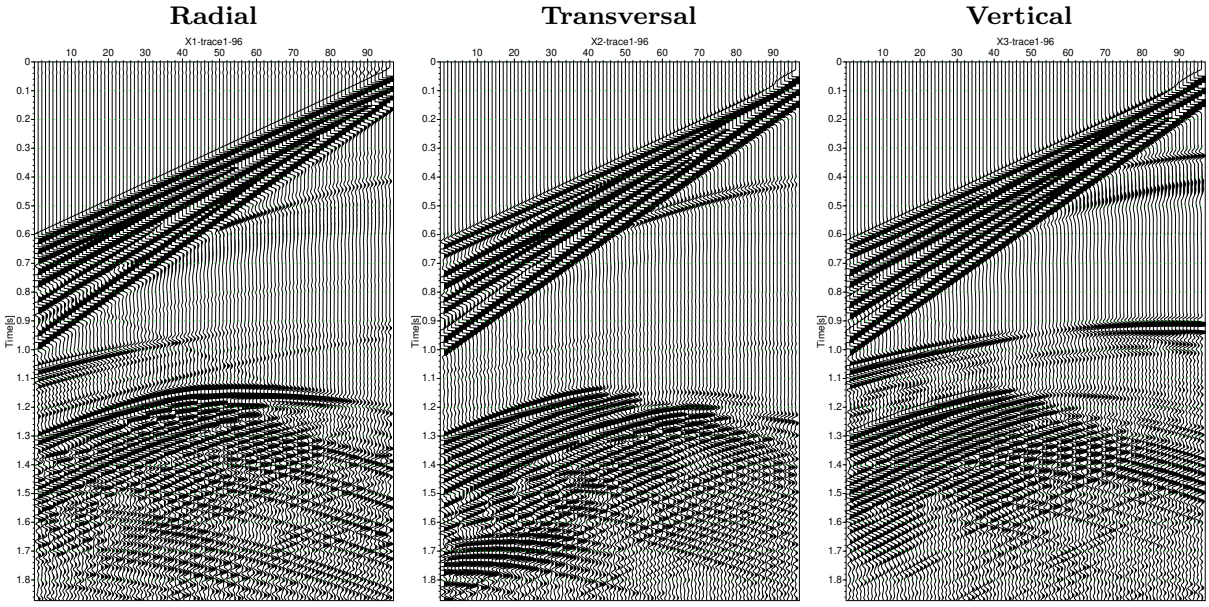

Figure 4. Radial (X1), transversal (X2) and vertical (X3) components of the complete wave field for common-shot gather 1. The complete seismic wave field is calculated using the Fourier pseudospectral method in the velocity model with the triclinic anisotropy in the upper layer.

During our migration tests with ray-theory P, S1, S2 reflected and converted waves calculated in the same model with triclinic anistropy, we observed receivers experiencing a change in the sign of the reflection coefficient around a region of the nearly vanishing reflection coefficient (Bucha, 2018a). This is caused by the fact that the value of the corresponding elementary wave velocity in the isotropic bottom layer is between the values of the horizontal (axis x_1) and vertical (axis x_3) wave velocities in anisotropic upper layer (for details, please refer to Bucha, 2017). The same effect we observe for the complete wave field calculated using the Fourier pseudospectral method (see Figure 4 vertical component near time 1 s).

Figure 5 displays migrated sections of PP reflected wave. The migrated interface for radial and transversal components is invisible. Big part of migrated interface for vertical component (X3) is composed of pieces with erroneous rotation. To exclude the influence of nearly vanishing reflection coefficient we increased the P-wave velocity in the bottom layer from $V_p = 3.6$ km/s to $V_p = 3.8$ km/s and calculated new complete wave field and performed migration. Migrated interface is a little bit better focused and the part in the horizontal range of approximately 2–4 km is now visible.

Stacked migrated sections for three components of PS1 converted wave are presented in Figure 6. We obtain the best result for radial component. The migrated interface for transversal and vertical components is imaged only partially. The quality of migrated sections for PS2 converted wave (Figure 7) is similar to PS1 converted wave. However, for PS1 wave we get the best imaged interface for transversal component while for radial and vertical components the migrated interfaces are visible only partially. To exclude the influence of nearly vanishing reflection coefficient we apply for all components the test with increased P-wave velocity in the bottom layer from $V_p = 3.6$ km/s to $V_p = 3.8$ km/s. Nevertheless, the migrated sections are nearly the same for both cases and we do not display them.

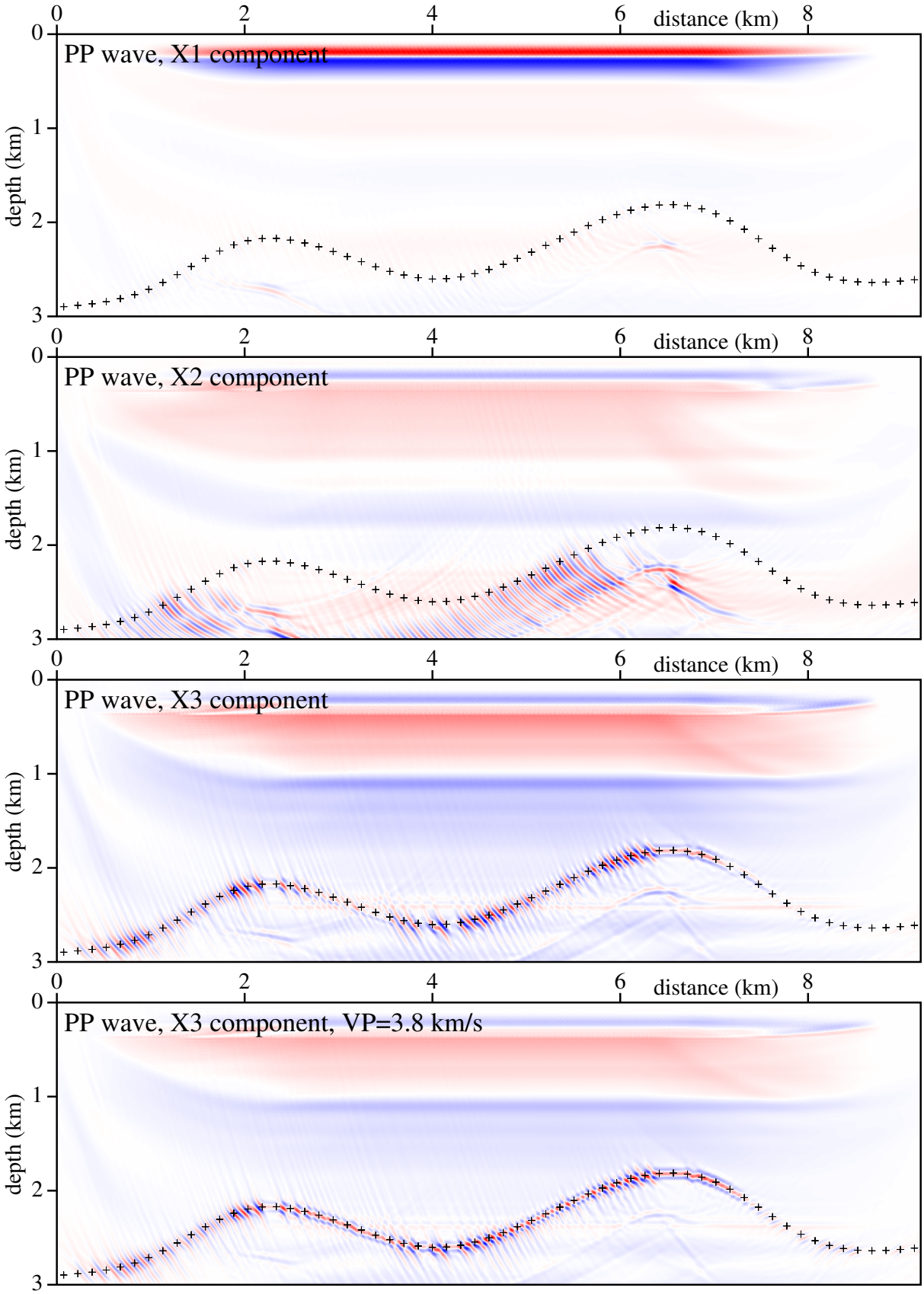

Figure 5. Stacked migrated sections calculated in the triclinic velocity model without interface. Radial (X1), transversal (X2) and vertical (X3) components of PP reflected wave are used. 81×240 common-shot prestack depth migrated sections, corresponding to 81 profile lines and 240 sources along each profile line, have been stacked. The crosses denote the interface in the velocity model used to compute the recorded wave field.

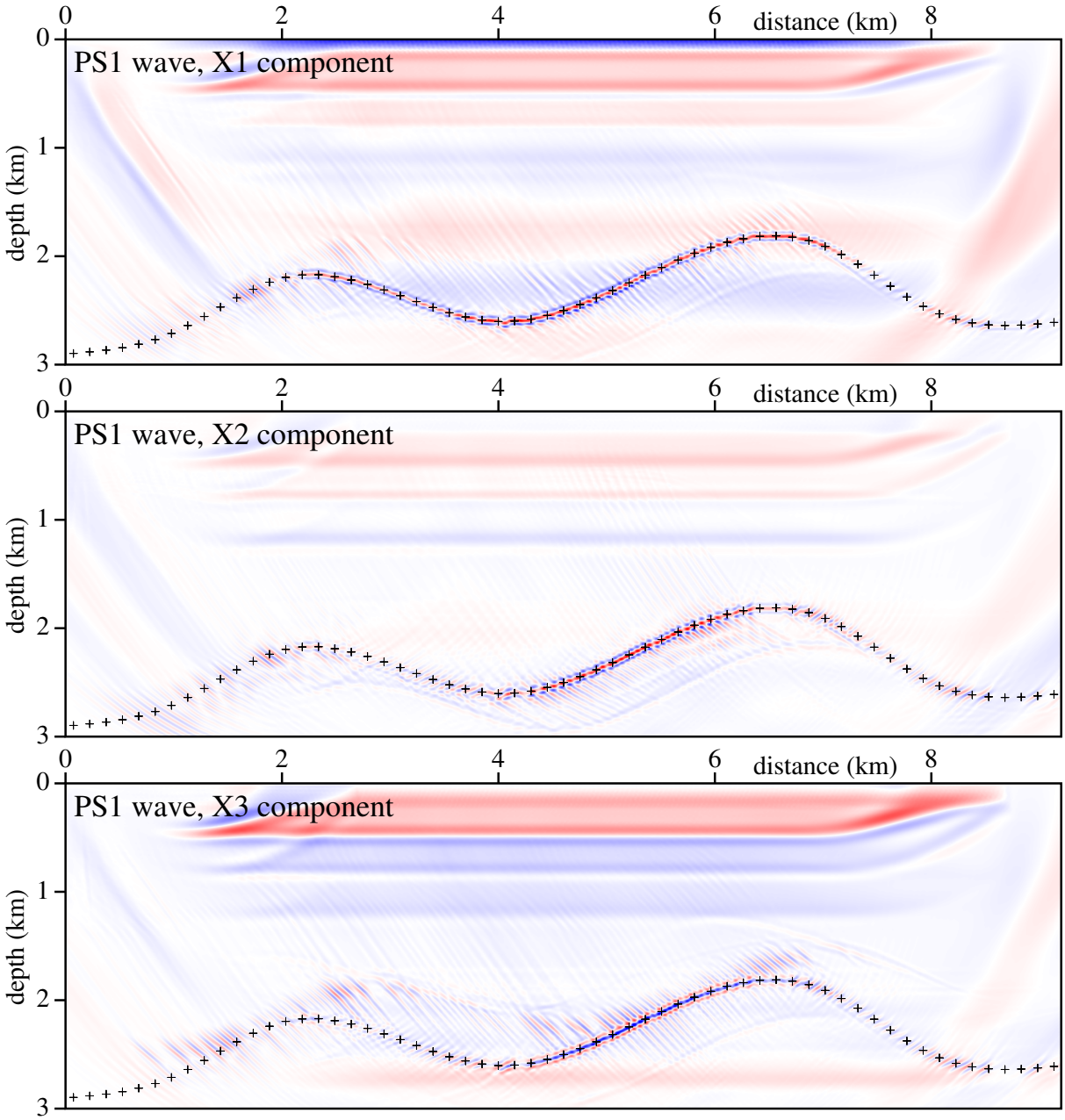

Figure 6. Stacked migrated sections calculated in the triclinic velocity model without interface. Radial (X1), transversal (X2) and vertical (X3) components of PS1 converted wave are used. 81×240 common-shot prestack depth migrated sections, corresponding to 81 profile lines and 240 sources along each profile line, have been stacked. The crosses denote the interface in the velocity model used to compute the recorded wave field.

In Bucha (2019a) we imaged only vertical component of PP reflected wave, radial component of PS1 converted wave and transversal component of PS2 converted wave in inhomogeneous weekly anisotropic models QI and QI4. Comparison of analogous migrated sections shows that migrated sections for models QI and QI4 are much more better imaged than for homogeneous triclinic model used in this paper.

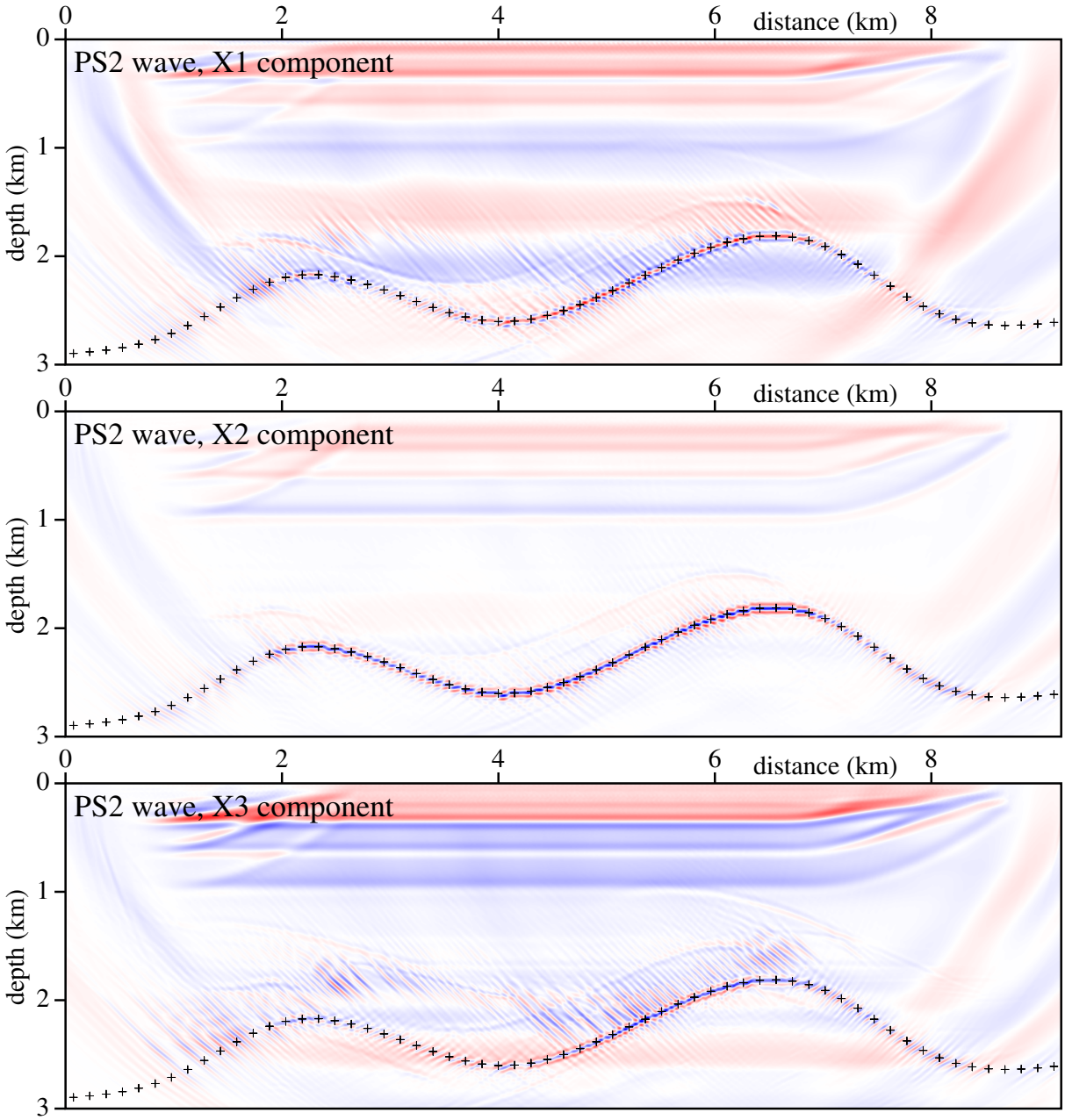

Figure 7. Stacked migrated sections calculated in the triclinic velocity model without interface. Radial (X1), transversal (X2) and vertical (X3) components of PS2 converted wave are used. 81×240 common-shot prestack depth migrated sections, corresponding to 81 profile lines and 240 sources along each profile line, have been stacked. The crosses denote the interface in the velocity model used to compute the recorded wave field.

5. Spurious oblique strips in the migrated sections

Since the recorded wave field is not decomposed into the P, S1 and S2 waves, parts of the recorded P wave are migrated as the S1 or S2 waves, and parts of the recorded S1 and S2 waves are migrated as the P wave. The corresponding false images are sometimes reduced by the destructive interference (Bucha, 2019a), but sometimes not. The false images of some parts of the interface can be observed in Figures 5, 6 and 7.

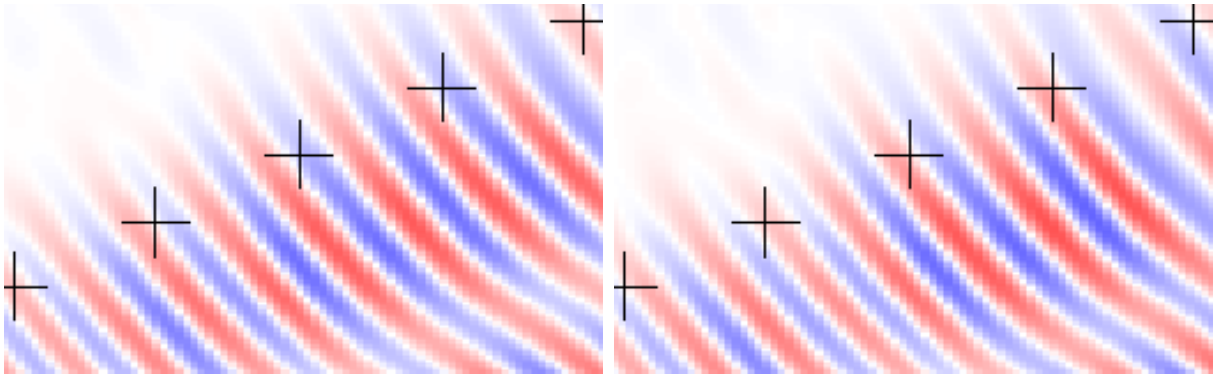

Figure 8. Details of the stacked migrated sections for the transversal (X2) component of the PP reflected wave. The left-hand detail corresponds to Figure 5, while the right-hand detail corresponds to the migrated section calculated for the complete recorded wave-field computed with the grid shifted by 12.5 m upwards. Note the exchange of the red and blue strips with respect to the crosses.

When calculating the recorded wave field, the originally smooth interface is approximated by the stair-step interface with the vertical step of 0.025 km. The stair-step interface is clearly visible in Figure 7 (middle section), and to a small extent also in Figure 6 (top section) and other two sections of Figure 7.

In Figure 5 (X2 component), we observe pronounced oblique strips. The strips are probably caused by the S-wave diffractions at the edges of the stair-step interface back-propagated as a P wave. In order to verify this hypothesis, we shifted the grid for calculating the recorded wave field vertically by 0.0125 km. The newly created edges of the stair-step interface are located approximately between the former edges. The oblique strips due to the new edges have approximately opposite signs than the strips due to the old edges, which is clearly visible in the details displayed in Figure 8. Less pronounced oblique strips are present in Figure 5 (X3 component), in Figure 6 and in Figure 7 (X1 and X3 components).

6. Conclusions

We calculated complete wave fields in a simple two-layer velocity model composed of two homogeneous layers with relatively strong triclinic anisotropy in the upper layer. We then applied the 3-D ray-based Kirchhoff prestack depth scalar migration to the homogeneous single-layer velocity model with the same triclinic anisotropy. We migrated radial, transversal and vertical components of PP reflected wave, PS1 and PS2 converted waves. S1 and S2 parts of converted waves were computed using anisotropic-ray-theory method. The migrated sections are much worse than analogous migrated sections calculated for inhomogeneous weekly anisotropic models QI and QI4 presented in Bucha (2019a). The effect of the stepwise discretization of the smooth interface during the forward modelling on the migrated sections will further be studied.

Acknowledgements

The author thanks Ekkehart Tessmer for providing the Fourier method code. The author also thanks Ivan Pšenčík and Luděk Klimeš for their help throughout the work on this paper.

The research has been supported by the Czech Science Foundation under Contract 20-06887S, and by the members of the consortium "Seismic Waves in Complex 3-D Structures" (see "http://sw3d.cz").

References

Bucha, V. (2012): Kirchhoff prestack depth migration in 3-D simple models: comparison of triclinic anisotropy with simpler anisotropies. *Stud. geophys. geod.*, **56**, 533–552.

Bucha, V. (2013): Kirchhoff prestack depth migration in velocity models with and without vertical gradients: Comparison of triclinic anisotropy with simpler anisotropies. In: *Seismic Waves in Complex 3-D Structures*, **23**, 45–59, online at "http://sw3d.cz".

Bucha, V. (2017): Kirchhoff prestack depth migration in simple models with differently rotated elasticity tensor: orthorhombic and triclinic anisotropy. *J. seism. Explor.*, **26**, 1–24.

Bucha, V. (2018a): Kirchhoff prestack depth scalar migration in a simple triclinic velocity model for three-component P, S and converted waves. In: *Seismic Waves in Complex 3-D Structures*, **28**, 61–84, online at "http://sw3d.cz".

Bucha, V. (2018b): Kirchhoff prestack depth scalar migration of complete wave field in a simple inhomogeneous weakly anisotropic velocity model: preliminary tests. In: *Seismic Waves in Complex 3-D Structures*, **28**, 85–96, online at "http://sw3d.cz".

Bucha, V. (2019a): Kirchhoff prestack depth scalar migration of complete wave fields in simple inhomogeneous weakly anisotropic velocity models: PP, PS1 and PS2 waves. In: *Seismic Waves in Complex 3-D Structures*, **29**, 19–38, online at "http://sw3d.cz".

Bucha, V. (2019b): Kirchhoff prestack depth scalar migration of a complete wave field: stair-step interface. In: *Seismic Waves in Complex 3-D Structures*, **29**, 39–44, online at "http://sw3d.cz".

Bucha V. and Bulant P. (eds.) (2019): SW3D-CD-23 (DVD-ROM). *Seismic Waves in Complex 3-D Structures*, **29**, 71–72, online at "http://sw3d.cz".

Bulant, P. (1996): Two-point ray tracing in 3-D. *Pure appl. Geophys.*, **148**, 421–447.

Bulant, P. (1999): Two-point ray-tracing and controlled initial-value ray-tracing in 3-D heterogeneous block structures. *J. seism. Explor.*, **8**, 57–75.

Bulant, P. & Klimes, L. (1999): Interpolation of ray-theory travel times within ray cells. *Geophys. J. int.*, **139**, 273–282.

Bulant, P. & Klimeš, L. (2008): Numerical comparison of the isotropic-common-ray and anisotropic-common-ray approximations of the coupling ray theory. *Geophys. J. Int.*, **175**, 357–374.

Bulant, P., Pšenčík, I., Farra, V. & Tessmer, E. (2011): Comparison of the anisotropic-common-ray approximation of the coupling ray theory for S waves with the Fourier pseudo-spectral method in weakly anisotropic models. In: *Seismic Waves in Complex 3-D Structures*, **21**, 167–183, online at "http://sw3d.cz".

Cerjan, C., Kosloff, D., Kosloff, R. & Reshef, M. (1985): A non-reflecting boundary condition for discrete acoustic and elastic wave calculation. *Geophysics*, **50**, 705–708.

Červený, V., Klimeš, L. & Pšenčík, I. (1988): Complete seismic-ray tracing in three-dimensional structures. In: Doornbos, D.J. (ed.), *Seismological Algorithms*, Academic Press, New York, pp. 89–168.

Cohen, J. K. & Stockwell, Jr. J. W. (2013): CWP/SU: Seismic Un*x Release No. 43R5: an open source software package for seismic research and processing, Center for Wave Phenomena, Colorado School of Mines.

Farra, V. & Pšenčík, I. (2010): Coupled S waves in inhomogeneous weakly anisotropic media using first-order ray tracing. *Geophys.J.Int.*, **180**, 405–417.

Klimeš, L. & Bulant, P. (2016): Prevailing-frequency approximation of the coupling ray theory for electromagnetic waves or elastic S waves. *Stud. geophys. geod.*, **60**, 419–450.

Klimeš, L. & Bulant, P. (2017): Interpolation of the coupling-ray-theory Green function within ray cells. *Stud. geophys. geod.*, **61**, 541–559.

Kosloff, D. & Baysal, E. (1982): Forward modeling by a Fourier method. *Geophysics*, **47**, 1402–1412.

Mensch, T. & Rasolofosaon, P. (1997): Elastic-wave velocities in anisotropic media of arbitrary symmetry-generalization of Thomsen's parameters ϵ, δ and γ. *Geophys. J. Int.*, **128**, 43–64.

Pšenčík, I. & Dellinger, J. (2001): Quasi-shear waves in inhomogeneous weakly anisotropic media by the quasi-isotropic approach: a model study. *Geophysics*, **66**, 308–319.

Pšenčík, I., Farra, V. & Tessmer, E. (2011): Comparison of the FORT approximation of the coupling ray theory with the Fourier pseudospectral method. In: *Seismic Waves in Complex 3-D Structures*, **21**, 129–166, online at "http://sw3d.cz".

Tessmer, E. (1995): 3-D seismic modeling of general material anisotropy in the presence of the free surface by a Chebychev spectral method. *Geophys. J. Int.*, **121**, 557–575.

Versteeg, R. J. & Grau, G. (eds.) (1991): The Marmousi experience. *Proc. EAGE workshop on Practical Aspects of Seismic Data Inversion (Copenhagen, 1990)*, Eur. Assoc. Explor. Geophysicists, Zeist.